Available online at www.sciencedirect.com

ScienceDirect

journal homepage: www.elsevier.com/locate/he

$La_{1-x}Ca_xAl_{1-y}Ni_yO_3$ perovskites used as precursors of nickel based catalysts for ethanol steam reforming

Fabiola N. Agüero [a,*], *Maria Roxana Morales* [a], *Sebastian Larrégola* [a], *Eduardo M. Izurieta* [b], *Eduardo Lopez* [b], *Luis E. Cadús* [a]

[a] *Instituto de Investigaciones en Tecnología Química (INTEQUI), UNSL – CONICET, Ejército de los Andes 950 Bloque 3 2do piso, 5700 San Luis, Argentina*

[b] *Planta Piloto de Ingeniería Química (PLAPIQUI), UNS – CONICET, Bahía Blanca, Argentina*

ARTICLE INFO

Article history:
Received 4 April 2015
Received in revised form
19 July 2015
Accepted 9 August 2015
Available online 9 October 2015

Keywords:
Perovskites
Nickel
Steam reforming
Ethanol

ABSTRACT

On the search of new design procedures for high performance catalysts we have obtained a very precisely defined surface architecture starting from a particular host structure. In this case, high purity $La_{1-x}Ca_xAl_{1-y}Ni_yO_3$ (x = 0, 0.1; y = 0.1, 0.2, 0.3) perovskites were chosen, prepared by the citrate method and evaluated in the ethanol steam reforming reaction. The samples were characterized by X-ray diffraction (XRD), specific surface area measurements, X-ray photoelectron spectroscopy (XPS), X-ray absorption near-edge structure (XANES) and extended X-ray adsorption fine structure (EXAFS), temperature-programmed reduction (TPR) and Hydrogen Chemisorption. All the samples presented an excellent catalytic activity and stability. Exceptionally high H_2 yield values and low CO and CH_4 selectivities were observed. Perovskite without the addition of Ca and with a value of y = 0.2 presented the highest stability during 12 h on stream.

Introduction

Ethanol steam reforming is an endothermic reaction that produces only hydrogen and carbon dioxide if ethanol reacts in the most desirable way. However, usually by-products such as carbon monoxide, methane, acetaldehyde and ethylene can be formed. The use of an appropriate catalyst must favour the reaction mechanism that reduces the formation of those by-products, increasing the selectivity to the main products. In general, different metals such as Ni [1], Co [2], Cu [3], Rh, Pt, Ru [4,5] deposited on oxides supports (Al_2O_3, La_2O_3, ZnO, MgO) have shown a good level of activity and selectivity for ethanol steam reforming. The high C–C bond breaking activity and the relatively low cost of Ni make it a suitable active phase for this reaction. However, there are still some challenges in the application of Ni based catalysts. One of them is to avoid Ni particle sintering, since large particles facilitate the formation of carbon leading to the deactivation of the catalyst [6]. The formation of carbonaceous deposits is a structure sensitive reaction, and thus controllable with the domain size of Ni centers. Beengard et al. [7], have reported a critical size below which the formation of coke can be prevented and additives such as K, S and Au catalyst can give more tolerance to carbon

* *Corresponding author.*
E-mail address: fnaguero@unsl.edu.ar (F.N. Agüero).
http://dx.doi.org/10.1016/j.ijhydene.2015.08.051

formation. According to a model proposed by Borowecki [8] there is a relationship between the domain size of the Ni catalytic center and the rate of formation of coke. Chen et al. [9] found that the crystal size of Ni has very significant effects on the carbon nanofibers growth, including the initial coking rate, the deactivation rate, and the final yield of carbon nanofibers.

Another challenge is to prevent carbon deposition, which takes place through the hydrogenation of CO and CO_2 at low temperatures and the decomposition of methane, ethane and ethylene at higher temperatures [10]. The use of high surface area supports favours the dispersion of active phase on the support pores. γ-Al_2O_3 is widely used as support, mainly due to its thermal and mechanical stability associated with a high surface area. However, its high acidity favors the reaction of ethanol dehydration, which can lead to a progressive deactivation of the catalyst [11]. Thus, the use of basic additives and promoters such as alkali metal and alkaline earth has been suggested as an alternative to neutralize the acid sites of the γ-Al_2O_3 [12,13]. Small amounts of MgO on Ni/Al_2O_3 catalysts caused a significant decrease in coke deposition in the steam reforming reaction due to the decrease of the support acidity [13]. Calcium is a metal with basic properties and has been used as additive by several researchers in steam reforming reactions. Choong et al. found an optimized Ca loading that play a critical role in coke removal [14]. Elias et al. studied the addition of Ca to Ni/Al_2O_3 catalysts and found that these catalysts presented the lowest acidity and carbon deposition and an excellent stability for 24 h of catalytic test [15]. Zhong et al. [16]. studied the role of acid sites on the catalytic steam reforming of ethanol using Rh catalysts supported on different types of ZrO_2. In order to modify the acid and basic properties of the support, the authors added small amounts of La_2O_3,CeO_2 and Al_2O_3. They found that at low temperature (300 °C), the Rh catalyst based on the La promoted ZrO_2 support with two types of acid sites was more active, while above 450 °C all the catalysts exhibited a similar catalytic activity.

Thus, it is essential to use a particular design criteria during the synthesis of catalysts, since the activity, selectivity and stability are affected by the nature of the metal particle, the support and the interaction between them. Therefore, it is necessary to make a proper selection of supports, either with the addition of alkali elements [17], with the use of supports with redox properties [18–20] or using novel methods of preparation [21] to modify their properties and their interaction with the nickel particles [22,23].

Perovskite oxides are widely used materials as catalysts. This structure, with general formula ABO_3 with A an alkaline or lanthanide cation and B a transition element, admits the inclusion by substitution of other cations A′ or B′. There are several articles that report the use of these oxides in ethanol steam reforming reactions, however, only few of them have demonstrated to obtain solids with high purity [24–26]. The main advantage of this type of structure is given by the possibility of its destruction by a reduction procedure. Thus, an in situ formation of a phase arrangement appropriate to obtain stable and active catalysts for the studied reaction is possible only with the use of high purity solids. Therefore, the objective of this work is to obtain pure AA'BB'O_3 perovskites as catalysts precursors with a correct selection of the cations in order to generate in situ the active phase and the support with suitable features for the ethanol steam reforming reaction.

Experimental

Catalysts preparation

$La_{1-x}Ca_xAl_{1-y}Ni_yO_3$ (x = 0, 0.1; y = 0, 0.1, 0.2, 0.3) perovskites were prepared by the citrate method [27]. $La(NO_3)_3 \times 6H_2O$, $Ca(NO_3)_2 \times 4H_2O$, $Al(NO_3)_3 \times 6H_2O$, $Ni(NO_3)_2$ were dissolved in water and were added to an excess citric acid solution. The resulting solution was slowly evaporated under vacuum in a rotavapor at 75 °C until a gel was obtained. This gel was dried in a vacuum oven, slowly increasing the temperature to 200 °C and maintaining this temperature overnight, to produce a solid amorphous citrate precursor. The resulting precursor was milled and then calcined in air at 800 °C for 2 h. The samples were named LaNiy and LaCaNiy with y = 1,2,3. Additionally, a NiO/$LaAlO_3$ catalyst was also prepared as reference by impregnation to incipient wetness with an aqueous solution of $Ni(NO_3)_2$. The amount of added solution was the necessary to obtain a nickel loading equivalent to LaNi1 catalyst.

Catalysts characterization

BET specific surface area measurements (SBET)
The specific surface area of the samples was calculated by the BET method from the nitrogen adsorption isotherms obtained at 77 K. A Gemini V from Micromeritics apparatus was used.

X-ray diffraction (XRD)
XRD patterns were obtained by using a Rigaku diffractometer operated at 30 kV and 25 mA by employing Cu Kα radiation with Nickel filter (λ = 0.15418 nm).

Inductively coupled plasma
The elemental composition was determined by inductively coupled plasma. An ELAN DRC-e ICP-MS apparatus was used. In each experiment, 10 mg of each catalyst was dissolved in 1 M HNO_3 solution with a START D Microwave Digestion System.

X-ray photoelectron spectroscopy (XPS)
XPS data were obtained with a Multitecnic UniSpecs equipment with a dual X-ray source of Mg/Al and an hemispheric analyzer PHOIBOS 150. A pass energy of 30 eV and an Al anode operated at 100 W was used. The pressure was kept under 29×10^{-8} mbar. The samples were previously reduced at 600 °C in 50 mL/min^{-1} 5% of H_2/N_2 stream.

Temperature programmed reduction (TPR)
The TPR was performed in a quartz tubular reactor using a TCD as detector. Samples of 100 mg were used. The reducing gas was a mixture of 5 vol% H_2/N_2, at a total flow rate of 30 mL min^{-1}. The temperature was increased at a rate of 10 °C min^{-1} from room temperature to 700 °C.

Hydrogen chemisorption

The samples were previously reduced at 600 °C with 50 mL/min of 5%H_2/Argon for1 h, followed by purging at 400 °C during 1 h. The H_2 isotherm was performed at 35 °C in a Micromeritics ASAP 2010 equipment.

XAFS

The XAFS experiments (including X-ray absorption near-edge structure region-XANES and extended X-ray adsorption fine structure region-EXAFS) were carried out at the XAFS2 beamline at LNLS, Campinas, Brazil [28], using a double crystal Si (111) monochromator. The Ni K-edge (8333 eV) spectra were collected in transmission mode. The required quantity of powder sample was mixed with boron nitride and pressed into self-supporting discs in order to obtain an homogeneous sample optimized for transmission measurements. The energy calibration was obtained by simultaneous absorption measurements on the Ni metal sample positioned between the second and the third ionization chamber. X-ray absorption data were analyzed by using standard procedures [29]; a linear background was fitted at the pre-edge region and then subtracted from the entire spectrum; the jump of the spectrum was normalized to unity with the post edge asymptotic value by using a quadratic fit. The atomic background, $\mu_0(k)$, was determined by using cubic splines and the radial distribution function FT (χ (k)) was obtained by Fourier transforming the k^3 weighted experimental XAFS (χ (k)) function in the region of 2–17 $Å^{-1}$, multiplied by A Hanning window, into the R space. The spectra reported represent the average of three data sets.

Catalytic tests

The catalytic evaluation of the prepared catalysts was accomplished in a lab-ioniscale kinetic set-up which includes dosing and evaporation of the liquid feed mixture (water + ethanol), electrical heating, and quantitative analysis of the exit gaseous stream (both composition and total volumetric flowrate were measured). The liquid feed was dosed by a syringe pump (Cole Parmer 74900) directly from a storage tank. The subsequent vaporization and overheating of this mixture was performed by using heating tapes. A furnace (Heraeus) with PID temperature control was employed to house a stainless steel reactor in which the catalyst was disposed. A K-type thermocouple was used to register the reactor temperature. The condensable fraction of the stream exiting the reactor was collected in a second storage tank, whereas non-condensables were quantified by GC (HP 4890D) equipped with Porapak Q and Carbosienve-II columns and a TCD detector. Additionally, the total volumetric flowrate of this gaseous fraction was measured by a bubble-soap meter in order to close element mass balances.

To fill the reactor, prepared catalysts were grounded up to a mean particle diameter of 0.4 mm. In order to moderate thermal effects, dilution by mixing with quartz (similar particle diameter) was adopted. 50–150 mg of catalyst were used, with a ratio catalyst:inert 1:10 w/w. The samples were previously reduced at 600 °C with 50 mL/min of 5%H_2/N_2 for1 h, followed by purging at the same temperature with 50 mL/min^{-1} of He during 30 min. By means of the above-described lab set-up, steady-state stability tests of the catalysts were performed operating at isothermal and isobaric conditions. Catalytic runs were conducted at 600 °C and 1.2 bar. A Water:ethanol feed molar ratio of 5:1 was selected (S/C = 2.5) with a WHSV 3.3×10^{-4} mLliq/(mgcatxmin) and using 50 mL/min of nitrogen as carrier.

Ethanol conversion (X_{EtOH}), Selectivity to carbon products (Sj) and hydrogen yield ηH_2 were estimated as:

$$X_{EtOH}\ (\%) = 100 \cdot (F_{EtOH,in} - F_{EtOH,out})/(F_{EtOH,in})$$

$$\eta_{H2}\ (\%) = 100 \cdot F_{H2,out}/(6 \cdot F_{EtOH,in})$$

$$S_j\ (\%) = 100 \cdot F_{j,out}/(\Sigma\ F_{j,out}),\ \text{with j} = CH_4,\ CO \text{ and } CO_2$$

Results

Specific surface area (S_{BET})

S_{BET} results are listed in Table 1. Perovskites substituted with Ca presented higher specific surface areas (12–17 $m^2\ g^{-1}$) than unsubstituted ones (around 6 $m^2\ g^{-1}$).

X-ray diffraction (XRD)

XRD patterns of LaNiy and LaCaNiy (y = 1,2,3) are shown in Fig. 1. All the samples showed a good crystallinity and presented a diffraction pattern close to the reported for the pure perovskite $LaAlO_3$ phase (JCPDS file 31-22). Diffraction lines corresponding to segregated phases of lanthanum, calcium, aluminium or nickel oxides were not observed. The crystallinity was not modified with the replacement of Ca in the A position, nor by the higher Ni content in the B position. The crystal structure was refined applying the Rietveld method to the XRD data. Due to the strong pseudo-cubic nature of the sample the refinement was carried out assuming a cubic Pm-3m perovskite structure (Fig. 2). The lattice parameter a increases linearly with the substitution of Al with Ni. The increase in the lattice parameter could be related with two different issues: First the differences between the ionic radii of Al^{3+}: 0.53 Å Ni^{3+}: 0.56 Å and Ni^{2+}: 0.8 Å and by the other way

Table 1 – BET specific surface area (m^2/g), elemental composition from ICP-OES (wt%) and Ni dispersion (%) from H_2 chemisorption.

Catalyst	SBET (m^2/g)	Ni content (wt%)		Exposed surface (m^2/g)
		Experimental	Nominal	
$Ni/LaAlO_3$	17.1	3.4	2.7	0.50
LaNi1	6	4	2.7	0.34
LaNi2	7	5.5	5.3	0.60
LaNi3	6	8.7	7.8	0.14
LaCaNi1	17	2.3	2.8	0.16
LaCaNi2	15	3.5	5.5	0.29
LaCaNi3	12	5.2	8.2	0.24

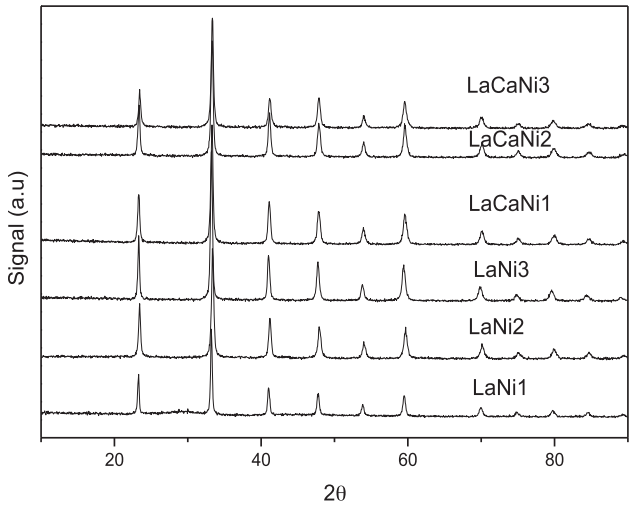

Fig. 1 – XRD patterns of LaNiy and LaCaNiy perovskites (y = 1, 2, 3).

with the possible generation of oxygen vacancies. These ones could be related with tendency of nickel to stabilize the Ni^{2+} oxidation state instead of Ni^{3+}, as it has been demonstrated for other perovskites, since high oxygen pressures are needed to keep the Ni^{3+} cation [30]. It is worth mentioning that the addition of Ca decreases the cell parameter of $LaAlO_3$ perovskite; quite possibly related with the inclusion of a smaller cation at the A-sublattice.

Inductively coupled plasma-optical emission spectroscopy

Table 1 summarizes the Ni content, expressed as weight percentage, of the synthetized catalysts. Ni content is lower than the nominal values in Ca substituted samples; however, the results of unsubstituted catalysts are similar to nominal values. However, the impregnated sample presents higher Ni content values than the perovskite sample with the same level of Ni substitution, (LaNi1).

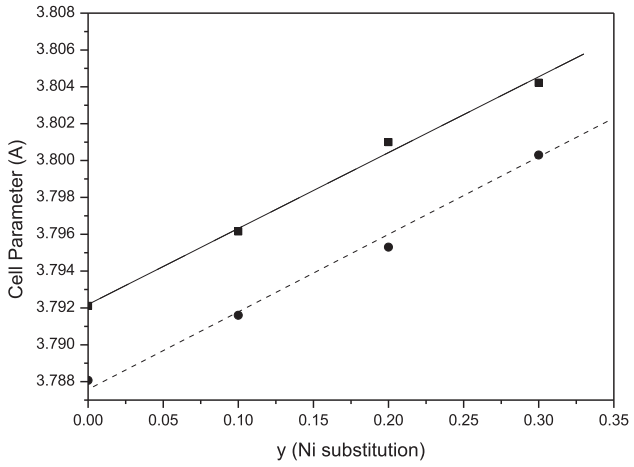

Fig. 2 – Lattice parameter vs y (Ni substitution). ■ LaNiy and ● LaCaNiy perovskites.

X-ray photoelectron spectroscopy (XPS)

The XPS data of the reduced catalysts are presented in Table 2, and are expressed as atomic ratios of the elements. Due to the existence of a partial overlapping between the $La3d_{3/2}$ and $Ni2p_{3/2}$ energy regions, it is difficult to estimate accurately the Ni oxidation state. However, the peak deconvolution allowed calculating the area of Ni2p and therefore quantitative measurements were performed. Ni/La + Ca + Al atomic ratio for the different Ni substitution levels in samples without calcium resulted higher than those of Ca substituted samples. It is also observed that Ni/La ratio keep almost constant while Ni/Al ratio increase with the increase of Ni content. These results could indicate that Ni after the reduction step is preferentially located on Al atoms. The decrease in La/Al ratio values with the addition of Ni in calcium substituted perovskites could indicate that Ca is placed on La atoms considering also that Ca/La ratio increase with Ni content. Additionally, Ca/La + Al + Ni ratio are higher than the nominal value (0.05) indicating an enrichment of Ca on the catalyst surface. The O 1s spectrum of all samples presented a main peak at around 530–531 eV. By deconvoluting this peak, two components are distinguished, namely the low binding energy peak at 529.8–530.1 eV, ascribed to lattice oxygen, O_l, (O_2^{2-}) and the high binding energy peak 531.3 eV, assigned to surface adsorbed oxygen, O_{ad}, (O^{2-} or O^-), OH groups and oxygen vacancies [31]. The relative abundance of O_l and O_{ad} species are listed in Table 2. As expected, the most abundant component in all samples was the lattice oxygen. It is interesting to note that the $LaAlO_3$ base perovskite evidences the presence of oxygen vacancies, ($O_{ad}/O_l = 0.39$) that could result in interesting oxidation centres. The Ni inclusion decreases the oxygen vacancies while Ca does not affect the surface defects. O_{ad}/O_l ratio resulted similar for all the substituted catalysts and were around 0.2.

X-ray absorption near-edge structure (XANES) and extended X-ray adsorption fine structure (EXAFS)

The XANES region of the XAFS spectra collected for LaNi2 and LaCaNi2 was analyzed on the basis of a linear combination of the different and possible oxidation states of nickel in the studied compounds. It is known that without using a high oxygen pressure synthesis method nickel in this kind of perovskites tends to stabilize mixed oxidation states (2+/3+) and these two cases are not the exception.

In Fig. 3, the above mentioned XANES spectra and the corresponding to the standards Ni°, NiO and $LaNiO_{3-d}$ are shown. From there the shape of the pre-edge peak of metallic nickel is not observed at the samples, which show a pre-edge peak similar to that displayed by the $LaNiO_{3-d}$ perovskite, suggesting the absence of the metal in the studied samples. Moreover, from the linear combination fit, this assumption was confirmed suggesting the presence of Ni^{2+} and Ni^{3+} in both structures. As a rough approximation we can see a 65/35% ratio for the $LaNiO_{3-d}$/NiO contributions for both samples. These results are qualitative, since there are some small issues that does not allow the exact calculation of the content of both species. Although, these results are not completely accurate (the vacancy level of $LaNiO_{3-d}$ is not known and the

Table 2 – XPS results.

Catalyst	Ni/La + Ca + Al	Ni/La	Ni/Al	La/Al	Ca/La	Ca/La + Al + Ni	O_{ad}/O_l
$LaAlO_3$				0.7			0.39
LaNi1	0.05	0.2	0.07	0.38			0.35
LaNi2	0.09	0.28	0.13	0.48			0.4
LaNi3	0.09	0.23	0.17	0.75			0.26
LaCaNi1	0.04	0.14	0.07	0.52	0.2	0.18	0.22
LaCaNi2	0.05	0.16	0.1	0.3	0.62	0.11	0.19
LaCaNi3	0.08	0.23	0.16	0.27	0.71	0.10	0.25

crystal structure of NiO is different to the perovskite one) we can confirm the presence of $Ni^{2+/3+}$, being, quite possibly, Ni^{3+} the most abundant in the structure.

The Fourier transform of the Ni K-edge EXAFS signal (FT) gives a pseudo radial distribution function around Ni atoms. The FT spectra of LaNi2 and LaCaNi2 are shown in Fig. 4. The experimental data is depicted as the solid line, the best fit is depicted as dashed line and the main contributions corresponding to the different bond lengths are represented as dotted lines. The first main peak (from 1 to 2 Å) correspond to the first coordination sphere that is composed of different Ni–O bond lengths. Peaks from 2 to 4 Å correspond to single scattering contributions from first rare earths and Ni neighbours, as well as, from second O neighbours. This region is rich in structural information. The refinement was made assuming a cubic perovskite structure and the FEFF programme [32] was used to calculate the radial distribution functions. LaNi2 exhibited a first peak corresponding to a Ni–O bond with a distance of 1.6 Å and several peaks from 2 to 4 Å. These peaks could be fitted with Ni–La bond distance, which is the main contribution of the second and more intense peak at a distance of 3 Å and with the contribution of Ni–Al–O, Ni–O–Al–O and Ni–La–O bond distances in a lesser extent. LaCaNi2 sample exhibited also a first peak that could be attributed to a Ni–O bond distance and two high intensity peaks at 2.6 and 3 Å. The third peak could be fitted with Ni–La and Ni–Al–O bond distances. Regarding the second peak located at 2.6 A, there was no predicted signal associated with the perovskite model capable of fit it. By this way, it was necessary to use additional contributions corresponding to a NiO structure. Then, the second peak could be attributed to a Ni–Ni bond distance from that NiO phase.

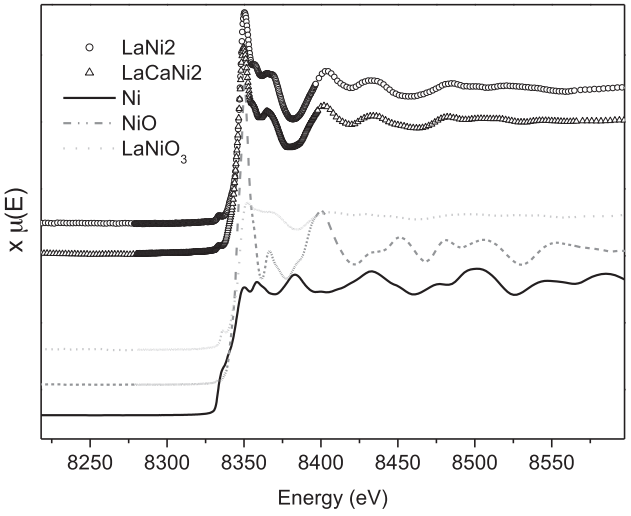

Fig. 3 – XANES spectra in the Ni K-edge region.

Temperature programmed reduction (TPR)

Fig. 5 shows the TPR profiles of all the catalysts. This figure also shows TPR results obtained for $Ni/LaAlO_3$, prepared by an impregnation method and $LaNiO_3$ perovskite taken as references. $LaNiO_3$ perovskite presents three reduction signals at around 350, 380 and 500 °C. It has been reported that the first two peaks are assigned to the reduction of $LaNiO_3$ to $La_4Ni_3O_{10}$ and then to La_2NiO_4. The third broad peak corresponds to the

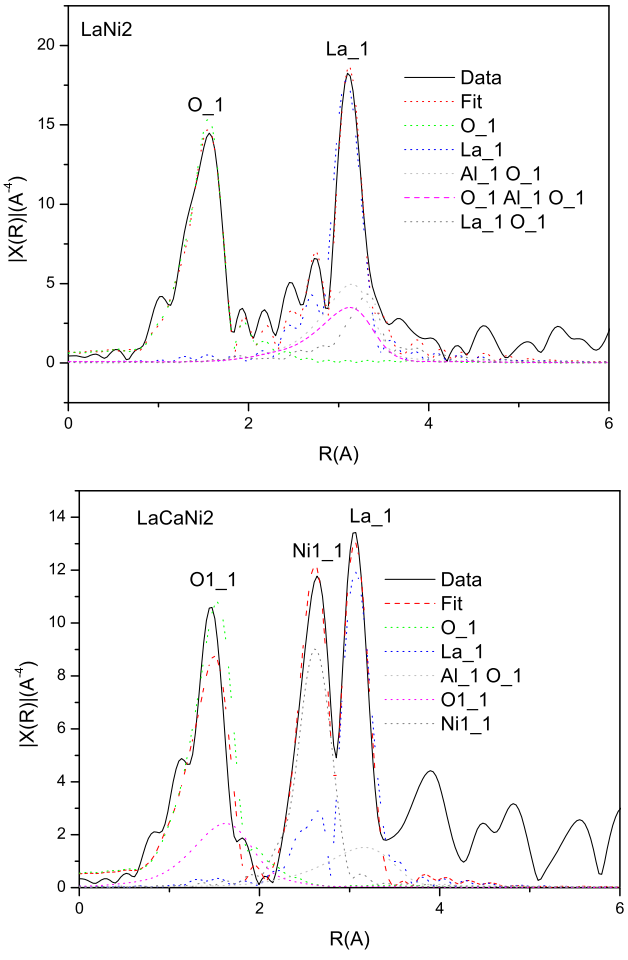

Fig. 4 – Fourier transform of the Ni K-edge EXAFS signal for a) LaNi2 and b) LaCaNi2.

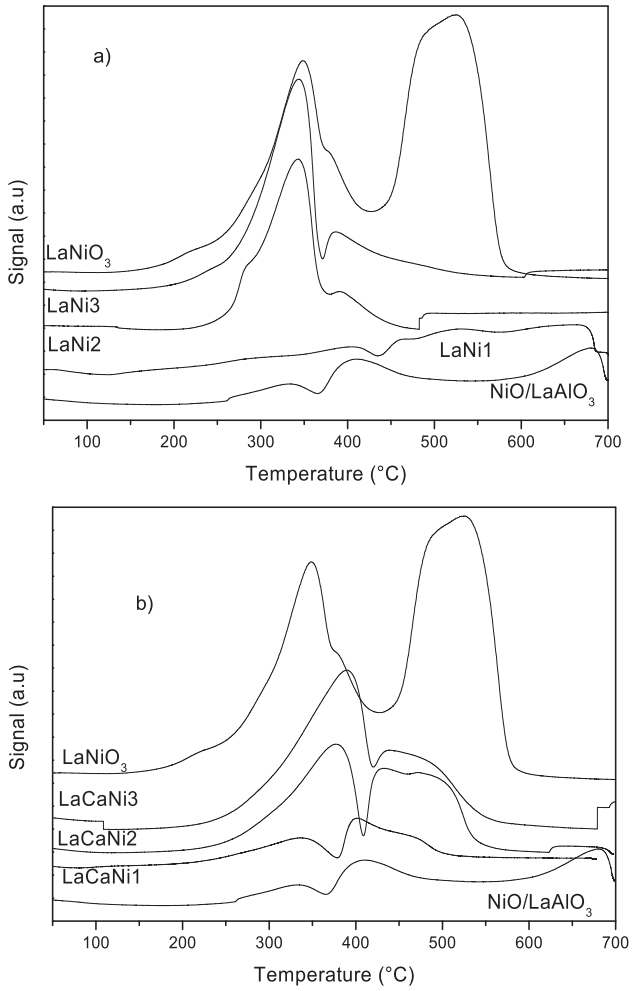

Fig. 5 – TPR profiles of a) LaNiy and b) LaCaNiy catalysts.

reduction of La_2NiO_4 to Ni° and La_2O_3 [33,34]. The reduction of $NiO/LaAlO_3$ occurs in two steps at around 330 and 420 °C. The perovskites prepared in this work present a main reduction signal at around 345 °C and signals with lower intensities between 380 and 500°. The intensity of these signals increases with the increase of Ni content. Calcium substitution evidences a shift of the reduction signals to higher temperatures and an intensity increase of the second and third signals. The overall appearance of the signals of the samples with calcium is quite similar to the one corresponding to the $NiO/LaAlO_3$ sample.

Hydrogen Chemisorption

The Ni exposed surface after the reduction treatment was estimated from the H_2 chemisorption results. It is worth mentioning that the dispersion of Ni on the surface can not be estimated from these results. Lower than real values would be obtained in perovskites since the amount of nickel available in the surface after the reduction treatment is lower than the total nickel content in the original perovskite structure. Metallic exposed surface results are shown in Table 1. There is not a direct relationship between Ni exposed surface and nickel substitution. LaNi2 catalyst, presents the highest metallic surface, 0.6 m^2/g. Calcium substituted samples present lower values than the unsubstituted ones, with the exception of LaCaNi3 which is higher than LaNi3. It is interesting to note that $NiO/LaAlO_3$ the sample prepared with an impregnation method presents a metallic surface of 0.5 m^2/g which is comparable to that of LaNi2 catalyst.

Catalytic performance

Fig. 6 presents the reaction performance of the catalysts as mean values from 6-hr on-stream catalytic tests under ethanol steam reforming. The performance parameters selected are ethanol conversion, hydrogen yield and CH_4, CO, and CO_2 selectivities. Total ethanol conversion was reached in all cases with exceptionally high values of H_2 yields, around 80%. Additionally, reduced CO and CH_4 selectivities were attained. The presence of acetaldehyde, ethane and ethylene, the most common precursors of carbon, were not detected in any case. Additionally, two catalysts (LaCaNi2 and LaNi2) were evaluated using one third of the catalyst weight used in the previous test. The stability of these samples was evaluated during 12 h on-stream. The corresponding results are reported in Fig. 7. The LaNi2 catalyst presented high stability with time–on-stream with total ethanol conversion along almost the whole test. H_2 yield remained about 80%, while low mean values of CH_4 and CO selectivities of 3.5 and 10%, respectively, were measured. Only after 10 h of reaction, a small amount of acetaldehyde was detected with the consequent drop in H_2 yield. LaCaNi2 also presented a good stability during 8 reaction hours with similar values of H_2 yield and CO, CO_2 and CH_4 selectivities as the LaNi2 sample. However, it started to deactivate slowly after that 8 h, decreasing the ethanol conversion and the H_2 yield to final values of 77 and 50%, respectively, at 12 reaction hours. Ethane, ethylene, acetaldehyde and unconverted ethanol were detected during this deactivation period.

The catalytic activity of a reference $Ni/LaAlO_3$ catalyst was also measured in the same operating conditions (1.5 h on-stream) in order to analyze the effect of the synthesis procedure (Fig. 6). The catalytic activity of this reference sample resulted considerable lower than that obtained with the perovskite catalysts. Ethanol conversion was incomplete from the beginning of the test and a maximum H_2 yield of only 35% could be attained. Not negligible amounts of acetone, acetaldehyde, ethane and ethylene were measured from the beginning of the experience, increasing with time-on-stream.

Discussion

The idea of studying a catalyst design lies in the need to find an active and selective catalyst with high stability in the steam reforming reaction. It is known that the necessary features to prevent catalyst deactivation are Ni particles with small domain sizes, with a high dispersion on a support with alkaline characteristics. Furthermore, the capability of the perovskite structure to incorporate several cations in a random way, generates islands enriched in different cations. The controlled destruction by a reduction step of the obtained pure disordered perovskite tends to move the most reducible

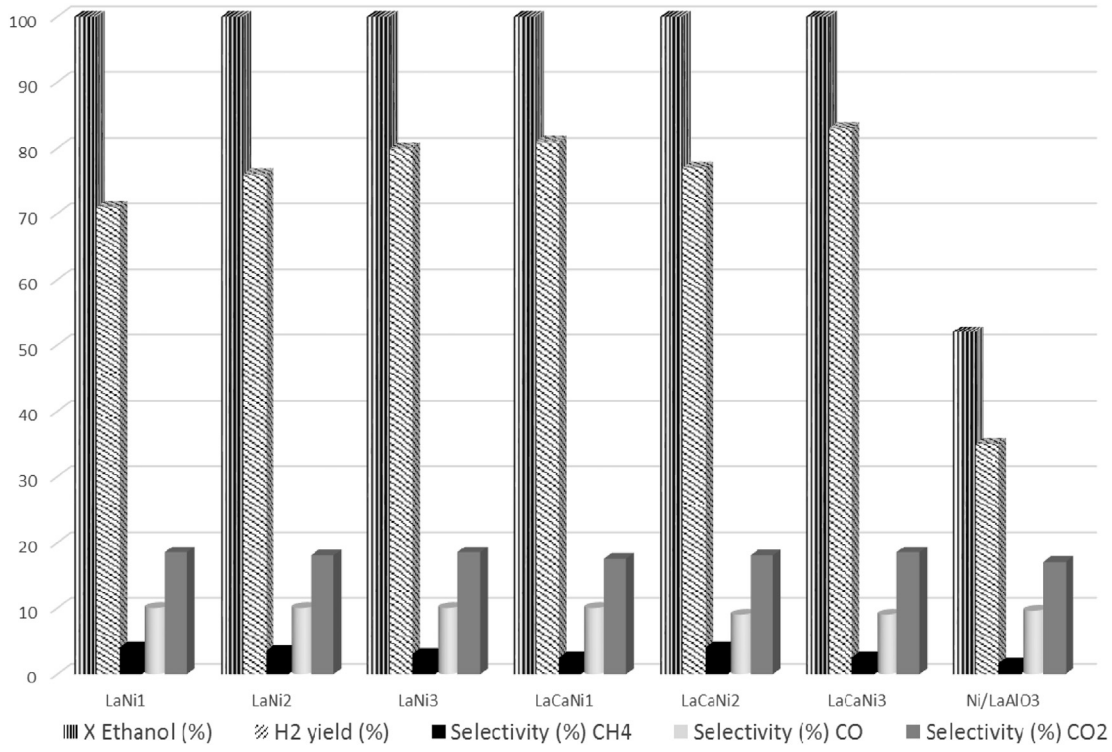

Fig. 6 – Catalytic activity results during 6 h on stream for perovskite catalysts and 1, 5 h for Ni/$LaAlO_3$ reference catalysts.

metal to the surface and generate small particles under the adequate conditions. By this way, the proposal of this work is to study perovskites as host structures of Ni and the subsequent generation of a catalyst with small metallic particles. The purity of the synthetized perovskites is essential in order to corroborate the inclusion of Ni in the structure and to control the expulsion of Ni after the reduction procedure. The samples in this work were prepared by the citrate method, which is recognized as an appropriate method to obtain pure solids since the precursor gel is highly homogeneous [35]. The success in the perovskite synthesis can be corroborated by X-ray diffraction (Fig. 1), where only a perovskite phase was observed. In no case, segregated phases of lanthanum, calcium, aluminum or nickel oxides were detected. However, the presence of these phases in very low concentrations or in an amorphous form can not be discarded due to the limitations of the technique. Considering, that Ni content in these perovskites is around 2–8% weight (Table 1), and the high crystallinity that these samples present, it could be deduced that the absence of diffraction lines corresponding to NiO phase could be related either to the presence of a small domain size of NiO or to the insertion of Ni into the perovskite structure. The increase in the cell parameter of the host perovskite, determined by a Rietveld refinement of the diffraction patterns (Fig. 2), would give evidence of the insertion of Ni. EXAFS technique is a useful tool to study the Ni environment in the structure. This is of great importance since it can allow us to corroborate the inclusion of this cation in the host perovskite and possibly the presence of nickel atoms with distinct environments. The information obtained from the Fourier transform of the Ni K-edge EXAFS signal (Fig. 4) of two of the catalysts prepared in this work (LaNi2 and LaCaNi2) confirm the inclusion of Ni in the structure of $LaAlO_3$ perovskite. The FT spectra of LaNi2 was fitted by using the contribution of the different bond distances corresponding to the perovskite structure. LaCaNi2 spectra also presented the contributions of the perovskite bond distances; however, an additional signal of a Ni–Ni bond distance corresponding to a NiO phase was also detected. TPR results presented in Fig. 5 give evidence of the previously stated. The presence of more than two signals would indicate the existence of a Ni^{3+}/Ni^{2+} phase. However the reduction signals of Ca-doped perovskites are quite similar to the one corresponding to the Ni/$LaAlO_3$, which could be indicating the segregation of NiO on these catalysts.

It is interesting to note, that the synthesis method is suitable since it is possible to obtain solids with acceptable specific surface areas rather than those prepared from ceramic methods. Merino et al. [36] studied $La_{1-x}Ca_xCoO_3$ perovskites and observed an important difference between the surface area of the unsubstituted and the substituted perovskites. In this paper similar results were obtained, the surfaces areas of substituted samples were almost the double of the corresponding to samples without calcium. Probably, the substitution of lanthanum with calcium changes the perovskite synthesis process, modifying the carboxilate precursor decomposition, and by this way, different textures are obtained. Even if the calcium replacement of lanthanum in the A sites is feasible because of the similarity between the ionic radii of the two species in 12-fold coordination (1.36 Å for La^{3+} and 1.34 Å for Ca^{2+} [37]), this replacement probably induces a structural disorder that leads to a delay in the crystallite growth. The selection of the degree of Ca substitution was made considering the results published in the literature. S.M. de Lima et al. [38] synthetized $La_{1-x}Ca_xNiO_3$ perovskites with

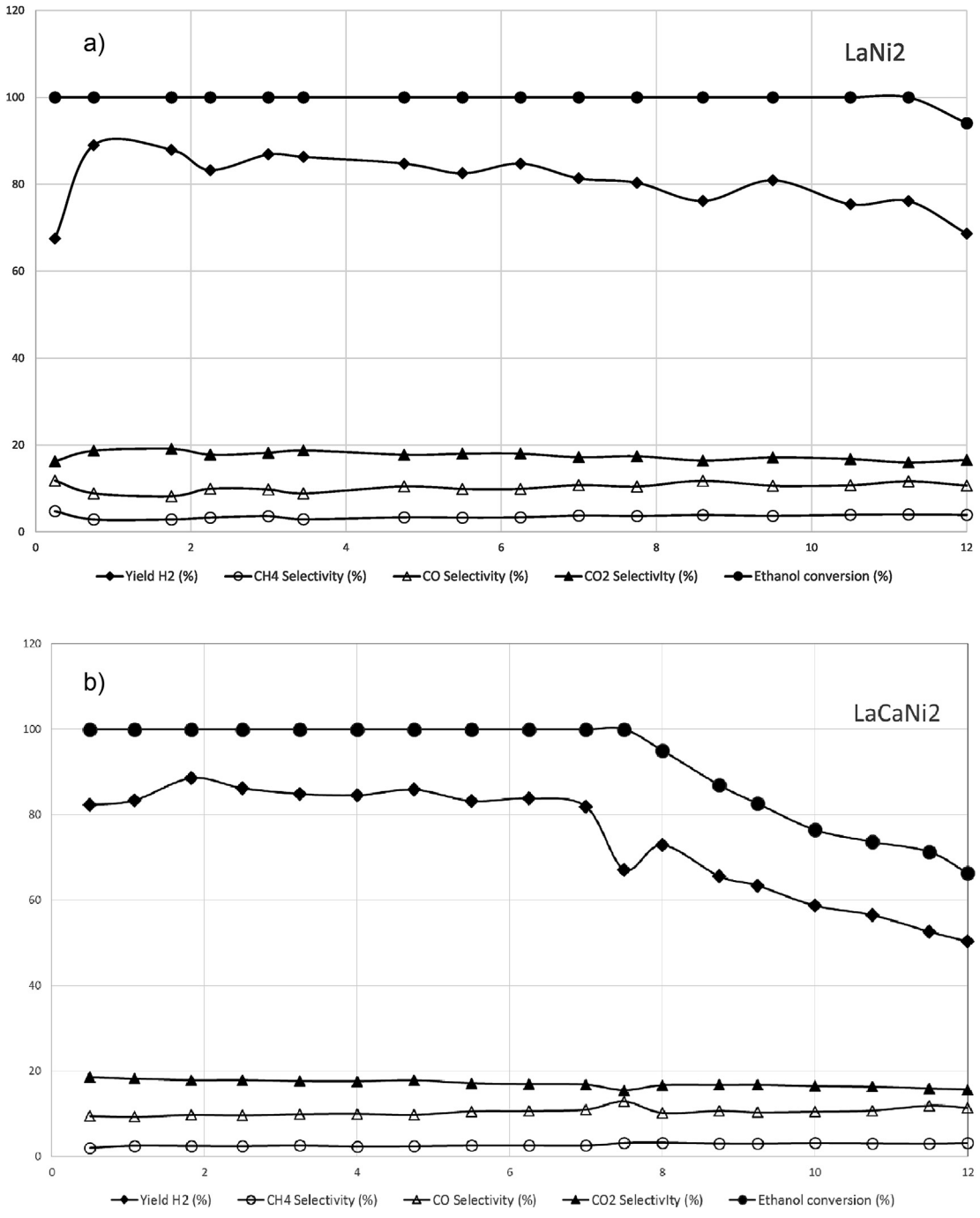

Fig. 7 – Stability test of a) LaNi2 and b) LaCaNi2 catalysts. (WHSV: 1×10^{-3} mLliq/(mgcatxmin)).

x: = 0, 0.05, 0.1, 0.3, 0.5, 0.8 used in partial oxidation of methane. They found a pure perovskite only with a substitution degree of 0.05. Above this value, they detected a segregation of oxides phases. A. Khalesi et al. [39] prepared $Ca_xLa_{1-x}Ni_{0.3}Al_{0.7}O_{3-d}$ and $Sr_xLa_{1-x}Ni_{0.3}Al_{0.7}O_{3-d}$ (x = 0, 0.2, 0.5, 0.8, and 1.0) perovskites catalysts for dry reforming of methane. With x > 0.2 they detected segregated phases beside the perovskite structure. Wu et al. [26] reported the synthesis of $La_{1-x}Ca_xNiO_3$ in glycerol steam reforming. For x = 1 the main phase detected was $LaNiO_3$ perovskite structure however the peak intensities decrease in comparison to the unsubtituted perovskite, and additional peaks were also detected simultaneously. Even if DRX results demonstrated a high purity of all the samples, EXAFS and TPR results give evidence of segregated NiO using even a x = 0.1 substitution level.

It is known that the active site in steam reforming reactions is metallic nickel, thus the expulsion of Ni to the surface was needed to generate the catalyst; this was carried out by a reduction procedure. TPR results show that all catalysts are completely reduced at 600 °C. Therefore, these samples were pretreated in a 5% H_2/N_2 stream at 600 °C during

1 h with a heating rate of 20 °C/min in the catalytic reactor. The catalytic performance of the prepared samples was evaluated in the ethanol steam reforming reaction in 6 h on-stream tests (see Fig. 6), attaining remarkable activity and stability values for all catalysts. Exceptionally high H_2 yields and low CO and CH_4 selectivities were observed. These results corroborate the success in the synthesis method employed. Certainly, a $NiO/LaAlO_3$ catalyst prepared by a simple impregnation method presented a very low activity and stability compared to perovskites with the same content of Ni. Wu et al. [26] observed a better catalytic performance in glycerol steam reforming on $La_{1-x}Ca_xNiO_3$ rather than Ni/La_2O_3. Batiot-Dupeirat et al. [40] also reported a higher catalytic activity on catalysts derived from $LaNiO_3$ perovskite type oxides than that on Ni/La_2O_3 prepared by the impregnation method in CO_2 reforming of CH_4. They attributed it to the stronger metal-support interaction and smaller Ni metallic particles on $LaNiO_3$ rather than Ni/La_2O_3. Evidently, the Ni expulsion to the surface in a controlled way generates Ni species with a higher performance than that generated from $NiO/LaAlO_3$. In fact, XPS results showed that Ni/La + Ca + Al atomic ratio for LaNi1 was 0.05, (Table 2) indicating that the expulsion of Ni is achieved in a controlled way repeating the atomic ratio of the crystalline lattice. Considering the higher metallic surface that the impregnated sample presents and the higher amount of atoms in the surface in comparison to that of LaNi1, the higher catalytic activity of perovskite probably would indicate that Ni species generated from the host structure would be smaller than the ones generated by impregnation.

The performance reached by all catalysts approaches the thermodynamic equilibrium, therefore only small differences in selectivity could be observed. Thus, in order to analyze the effect of Ca addition and seeking to operate with enhanced sensibility in the reaction performance parameters, it was decided to evaluate the catalysts farther from the equilibrium. Towards these ends, two catalysts (LaCaNi2 and LaNi2) were evaluated using one third of the weight used in the previous test (Fig. 7). Both catalysts presented an excellent catalytic performance in these conditions. LaNi2 catalyst presented high stability on time on stream with total ethanol conversion and 80% of H_2 yield with low mean values of CH_4 and CO selectivity. A small amount of acetaldehyde in the liquid effluent was detected only after 10 h of reaction. LaCaNi2 also presented a good stability during the first 8 h of reaction however, it started to deactivate slowly after that time decreasing the ethanol conversion and the H_2 yield at 12 reaction hours. Contrary to what it was expected the addition of an alkaline cation in this case does not favor the catalyst stability in spite of its high specific surface area and the presence of oxygen vacancies. A possible explanation to this issue could be related with the fact that the inclusion of both, Ni and Ca, is associated with the generation of oxygen vacancies. By this way, the inclusion of calcium generates enough vacancies to destabilize the perovskite structure (it is well known that the great stability of Pv structure is related with the 3D stacking of octahedra) so the nickel doping in the structure could be smaller in the case of LaCaNi samples than the doping degree of the LaNi ones. This fact is associated with the segregation of larger NiO particles, which has been suggested by the analysis of the TPR and XAFS data, and tends to deactivate in an easier way the catalysts with calcium, in an opposite way to the expected from the reported works where the inclusion of Ca or Mg improved the performance of the catalysts. Carrero et al. [41] studied the incorporation of alkaline-earth elements (Mg and Ca) to the silica support of $Cu–Ni/SiO_2$ catalysts used in ethanol steam reforming reaction. They found that both Mg and Ca addition improved the dispersion of the Cu–Ni metallic phase and strengthened metal–support interaction. Mg-promoted catalysts achieve the highest hydrogen selectivity. Evidently, one of the main factors affecting catalytic activity is the amount of Ni available at the surface of catalyst. It is known that the better the dispersion of nickel, the higher is the catalytic activity [42]. Mattos et al. [43] reported that the ethanol steam reforming requires a smaller quantity of metallic atoms assembled than the carbon formation reactions, so that smaller metal particles would lead catalysts with higher carbon formation resistance. In this case, XPS data show that Ca addition decreased the dispersion of Ni evidenced by the lower values of Ni/La + Ca + Al. H_2 chemisorption technique also corroborates the lower exposed surface of Ni on Ca substituted catalysts. The results showed up to now are in agreement with EXAFS data previously discussed. Evidently, and as we pointed out above, the absence of Ca favors the inclusion of Ni in the perovskite and therefore its reduction from a crystalline defined structure generates Ni species with higher activity in the steam reforming reaction. These results confirm the importance of preparing solids with high purity in order to achieve to active Ni species after the reduction treatment.

Conclusions

In the search of improved catalysts for the ethanol steam reforming reaction, we have developed a new design criterion based on the randomness nature of the cations disposition at the B-sublattice of simple perovskites. The consequent formation of nanoregions enriched in different cations plus the possibility of a controlled destruction of the structure allowed the segregation of highly interacted nanoparticles with a very promising conversion and selectivity in the reaction under study. $La_{1-x}Ca_x$-$Al_{1-y}Ni_yO_3$ (x = 0, 0.1; y = 0, 0.1, 0.2, 0.3) perovskites with appropriate textural features were prepared by the citrate method with high purity. The insertion of Ni in the perovskite structure was confirmed by the increase in the cell parameter of the host perovskite, and corroborated by the TPR and EXAFS results. All samples presented an excellent catalytic activity and stability during 6 h. Exceptionally high H_2 yield values and low CO and CH_4 selectivities were observed. The addition of Ca reduce the inclusion of Ni into the perovskite structure. A perovskite without the addition of Ca and with a value of y = 0.2 presented the highest stability during 12 on stream.

Acknowledgements

The financial support from Universidad Nacional de San Luis (Proy 2-0715-UNSL), Universidad Nacional de Sur, CONICET

(PIP N° 00080-CONICET), ANPCyT of Argentina (PICT Bicentenario-2010-2223 start up) and the LNLS (Pr. XAFS1 15968) is gratefully acknowledged. We thank to Prof. Gina Pechi from Universidad de Concepción, Chile, for the Hydrogen chemisorption measurements.

REFERENCES

[1] Fatsikostas AN, Kondarides DI, Verykios XE. Production of hydrogen for fuel cells by reformation of biomass-derived ethanol. Catal Today 2002;75:145–55.
[2] Llorca J, Homs N, Sales J, Ramirez de la Piscina P. Efficient production of hydrogen over supported cobalt catalysts from ethanol steam reforming. J Catal 2002;209:306–17.
[3] Mariño F, Boveri M, Baronetti G, Laborde M. Hydrogen production from steam reforming of bioethanol using Cu/Ni/K/γ-Al_2O_3 catalysts. Effect of Ni. Int J Hydrogen Energy 2001;26(7):665–8.
[4] Liguras DK, Kondarides DI, Verykios XE. Production of hydrogen for fuel cells by steam reforming of ethanol over supported noble metal catalysts. Appl Catal B Environ 2003;43(4):345–54.
[5] Navarro RM, Alvarez-Galván MC, Sanchez-Sanchez MC, Rosa F, Garcia Fierro JL. Production of hydrogen by oxidative reforming of ethanol over Pt catalysts supported on Al_2O_3 modified with Ce and La. Appl Catal B Environ 2005;55(4):229–41.
[6] Frusteri F, Freni S. Bio-ethanol, a suitable fuel to produce hydrogen for a molten carbonate fuel cell. J Power Sources 2007;173:200–9.
[7] Bengaard HS, Norskov JK, Sehested J, Clausen BS, Nielsen LP, Molenbroek AM, et al. Steam reforming and graphite formation on Ni catalysts. J Catal 2002;209:365–84.
[8] Borowiecki T. Nickel catalysts for steam reforming of hydrocarbons; size of crystallites and resistance to coking. Appl Catal 1982;4:223–31.
[9] Chen D, Chistensen KO, Ochoa-Fernadez E, Yu Z, Totdal B, Latorre N, et al. Synthesis of carbon nanofibers: effects of Ni crystal size during methane decomposition. J Catal 2005;229:82–96.
[10] Laosiripojana N, Assabumrungrat S. Catalytic steam reforming of ethanol over high surface area CeO_2: the role of CeO_2 as an internal pre-reforming catalyst. Appl Catal B 2006;66:29–39.
[11] Haryanto A, Fernando S, Murali N, Adhikari S. Current status of hydrogen production techniques by steam reforming of ethanol: a review. Energy Fuels 2005;19:2098–106.
[12] Lisboa JS, Santos DC, Passos FB, Noronha FB. Influence of the addition of promoters to steam reforming catalysts. Catal Today 2005;15:101–21.
[13] Viscaino AJ, Arena P, Baronetti G, Carrero A, Calles JA, Laborde MA, et al. Ethanol steam reforming on Ni/Al_2O_3 catalysts: effect of Mg addition. Int J Hydrogen Energy 2008;33:3489–92.
[14] Choong C, Zhong Z, Huang L, Wang Z, Peng Ang T, Borgna A, et al. Effect of calcium addition on catalytic ethanol steam reforming of Ni/Al_2O_3: I. Catalytic stability, electronic properties and coking mechanism. Appl Catal A 2011;407:145–54.
[15] Elias K, Lucrédito A, Assaf E. Effect of CaO addition on acid properties of Ni–Ca/Al_2O_3 catalysts applied to ethanol steam reforming. Int J Hydrogen Energy 2013;38:4407–17.
[16] Zhong Z, Ang H, Choong C, Chen L, Huang L, Lin J. The role of acidic sites and catalytic reaction pathways on the Rh/ZrO_2 catalysts for ethanol steam reforming. Phys Chem Chem Phys 2009;11:872–80.
[17] Frusteri F, Freni S, Chiodo V, Spadaro L, Di Blasi O, Bonura G. Steam reforming of bio-ethanol on alkali-doped Ni/MgO catalysts: hydrogen production for MC fuel cell. Appl Catal A 2004;270:1–7.
[18] Yang Y, Ma JX, Wu F. Production of hydrogen by steam reforming of ethanol over a Ni/ZnO catalyst. Int J Hydrogen Energy 2006;31:877.
[19] Biswas P, Kunzru D. Oxidative steam reforming of ethanol over Ni/CeO_2-ZrO_2 catalyst. Chem Eng J 2008;136:41–9.
[20] Sun J, Qiu XP, Wu F, Zhu WT. H_2 from steam reforming of ethanol at low temperature over Ni/Y_2O_3, Ni/La_2O_3 and Ni/Al_2O_3 catalysts for fuel-cell application. Int J Hydrogen Energy 2005;30:437–45.
[21] Sun G, Hidajat K, Kawi S. Synthesis of Y_2O_3 nanocrystals and the effect of nanocrystalline Y_2O_3 supports on Ni/Y_2O_3 catalysts for oxidative steam reforming of ethanol. Chem Lett 2006;35:1308–9.
[22] Orucu E, Gokaliler F, Aksoylu AE, Onsan ZI. Ethanol steam reforming for hydrogen production over bimetallic Pt–Ni/Al_2O_3. Catal Lett 2008;120:198–203.
[23] Srinivas D, Satyanara C, Potdar HS, Ratnasamy P. Structural studies on NiO-CeO_2-ZrO_2 catalysts for steam reforming of ethanol. Appl Catal A 2003;246:323.
[24] Cui Y, Galvita V, Rihko-Struckmann L, Lorenz H, Sundmacher K. Steam reforming of glycerol: the experimental activity of $La_{1-x}Ce_xNiO_3$ catalyst in comparison to the thermodynamic reaction equilibrium. Appl Catal B 2009;90:29–37.
[25] Franchini C, Aranzaes W, Duarte de Farías A, Pecchi G, Fraga M. Ce-substituted $LaNiO_3$ mixed oxides as catalyst precursors for glycerol steam reforming. Appl Catal B 2014;147:193–202.
[26] Wu G, Li S, Zhang Ch, Wang T, Gong J. Glycerol steam reforming over perovskite-derived nickel-based catalysts. Appl Catal B 2014;144:277–85.
[27] Courty P, Ajot H, Marcilly C, Delmon B. Oxydes mixtes ou en solution solide sous forme très divisée obtenus par décomposition thermique de précurseurs amorphes. Powder Technol 1973;7:21–38.
[28] Tolentino HCN, Ramos AY, Alves MCM, Barrea RA, Tamura E, Cezar JC, et al. A 2.3 to 25 keV XAS beamline at LNLS. J Synchrotron Rad 2001;8:1040–6.
[29] Teo BK. EXAFS basic principles and data analysis. Inorg. Chem. Conc, vol. 9. Berlin: Springer-Verlag; 1986.
[30] Kim S, Demazeau G, Alonso JA, Choy J. High pressure synthesis and crystal structure of a new Ni(III) perovskite: $TlNiO_3$. J Mat Chem 2001;11:487–92.
[31] Jiratova K, Mikulova J, Klempa J, Grygar T, Bastl Z, Kovanda F. Modification of Co–Mn–Al mixed oxide with potassium and its effect on deep oxidation of VOC. Appl Catal A 2009;361:106–16.
[32] Zabinsky SI, Reher JJ, Ankudinov A, Albers RC, Eller MJ. Multiple-scattering calculations of X-ray-absorption spectra. Phys Rev B 1995;52:2995.
[33] Gallego GS, Mondragón F, Barrault J, Tatibouët J-M, Batiot-Dupeyrat C. CO_2 reforming of CH_4 over La–Ni based perovskite precursors. Appl Catal A General 2006;311:164–71.
[34] Sierra Gallego G, Mondragón F, Tatibouët J-M, Barrault J, Batiot-Dupeyrat C. Carbon dioxide reforming of methane over La_2NiO_4 as catalyst precursor—characterization of carbon deposition. Catal Today 2008;133–135:200–9.
[35] Cifa F, Dinka P, Viparelli P, Lancione S, Benedetti G, Villa PL, et al. Catalysts based on $BaZrO_3$ with different elements incorporated in the structure I: $BaZr_{(1-x)}Pd_xO_3$ systems for total oxidation. Appl Catal B 2003;46:463–71.

[36] Merino NA, Barbero BP, Grange P, Cadús LE. $La_{1-x}Ca_xCoO_3$ perovskite-type oxides: preparation, characterisation, stability, and catalytic potentiality for the total oxidation of propane. J Catal 2005;231:232–44.
[37] Shannon RD. Revised effective ionic radii and systematic studies of interatomic distances in halides and chalcogenides. Acta Crystallogr Sect A 1976;32:751–67.
[38] de Lima SM, Peña MA, Fierro JLG, Assaf JM. Perovskites as catalyst precursors: partial oxidation of methane on $La_{1-x}Ca_xNiO_3$. Stud Surf Sci Catal 2007;167:481–6.
[39] Batiot-Dupeyrat C, Valderrama G, Meneses A, Martinez F, Barrault J, Tatibouët JM. Pulse study of CO_2 reforming of methane over $LaNiO_3$. Appl Catal A 2003;248:143–51.
[40] Khalesi A, Arandiyan HR, Parvari M. Effects of lanthanum substitution by strontium and calcium in La–Ni–Al perovskite oxides in dry reforming of methane. Chin J Catal 2008;29(10):960–8.
[41] Carrero A, Calles JA, Vizcaíno AJ. Effect of Mg and Ca addition on coke deposition over $Cu–Ni/SiO_2$ catalysts for ethanol steam reforming. Chem Eng J 2010;163:395–402.
[42] Tang S, Ji L, Lin J, Zeng HC, Tanand KL, Li K. CO_2 reforming of methane to synthesis gas over Sol–Gel-made $Ni/\gamma\text{-}Al_2O_3$ catalysts from organometallic precursors. J Catal 2000;194:424–30.
[43] Mattos LV, Jacobs G, Davis BH, Noronha FB. Production of hydrogen from ethanol: review of reaction mechanism and catalyst deactivation. Chem Rev 2012;112:4094–123.